Impact of Higher Current Harmonics on Component Current Stress and Conduction Losses of Half-Bridge-Series-Resonant-Converters in Discontinuous Conduction Mode for High-Power Applications

Daniel Haake[1], Anton Grodnichev[1], Fabian Schnabel[1], Marco Jung[1,2]

[1] Fraunhofer Institute for Energy Economics and Energy System Technology IEE
Joseph-Beuys-Straße 8
Kassel, Germany
Tel.: +49 561 7294 1589
daniel.haake@iee.fraunhofer.de
https://www.iee.fraunhofer.de/

[2] Hochschule Bonn-Rhein-Sieg
University of Applied Sciences
Grantham-Allee 20
Sankt Augustin, Germany
Tel. +49 2241 865 316
Marco.Jung@h-brs.de
https://www.h-brs.de

Acknowledgements

The authors acknowledge the support of the presented work by the German Federal Ministry for Economic Affairs and Climate Action within the project "MUSiCel: Mobile Umrichter und Energieübertragungslösungen auf SiC Basis für elektrische, leistungsstarke Land- und Baumaschinen" (FKZ 03EN2014E). Only the authors are responsible for the content of this publication.

Keywords

«DC power supply», «Isolated converter», «Resonant converter», «Silicon Carbide (SiC)», «ZCZVS converters»

Abstract

The half-bridge series resonant converter (HB-SRC) offers advantages with regard to power density compared to hard-switching topologies. To achieve soft-switching, the HB-SRC has to operate in discontinuous conduction mode (DCM). However, this operation influences component current waveforms and thus the component current stresses and losses in the converter, which are examined analytically and simulatively in this paper.

Introduction

Galvanically isolated DC-DC converters with high output power are used today in a wide variety of areas, from smart transformers in energy supply for AC and DC grids [1]-[3] to railway applications [4] and electrified agricultural machinery [5]. Series resonant converters (SRC) offer an advantage in achieving high power densities due to their low switching losses [5]. When silicon carbide power semiconductors are used, high switching frequencies can be achieved, which lead to an increase in power density. As shown in [1], [3]-[5], the half-bridge series resonant converter (HB-SRC) in discontinuous conduction mode (DCM), often referred to as half-cycle discontinuous-conduction-mode series resonant converter (HC-DCM-SRC [1], [3]), is particularly suitable due to the lower amount of required hardware in order to be able to implement the very compact systems with high performance. However, when the HB-SRC is operated to achieve soft switching, non-sinusoidal currents occur ([1], [3], [4]) which could lead to a massive increase in component current stress, particularly in high-power applications, and must therefore be taken into account throughout the design of the converter.

Soft switching Operation of the HB-SRC in DCM

The HB-SRC topology shown in Fig. 1 is examined. The associated waveforms of the currents and voltages in steady-state operation are shown in Fig. 2. For the following considerations, it is assumed that the input and output currents of the converter are approximately constant in steady-state operation. This applies, for example, in case that source and load of the HB-SRC are connected via inductances, for example through other converter stages [1] or sufficiently long cable connection [5].Furthermore, an energy flow from the HV-Side to the LV-Side is considered. It is also assumed that the transformer´s magnetization current i_{mag} is completely provided by the converter's HV-Side.
The HB-SRC topology (Fig. 1) consists of a primary-side half bridge with a split DC link at the converters input, a transformer, a resonance capacitance and a secondary-side full bridge, which is connected to the output capacitance of the converter. The equivalent circuit describing the transformer consists of an ideal transformer with the turn ratio N, a magnetizing inductance L_h, and a leakage inductance L_σ as described in [6]. The resonance tank of the HB-SRC is formed by the transformer's leakage inductance L_σ and the resonance capacitance C_{res}.
In the secondary-side full bridge, MOSFETs are used instead of diodes to allow a bidirectional power transfer through the converter. To reduce conduction losses, the full bridge works in synchronous rectification mode. The primary-side half bridge is controlled as described as follows. To ensure zero current switching (ZCS), the resonance frequency f_{res} is selected to be higher than the switching frequency f_{SW}, so that the resonant pulse of the current is completed before half the switching period is reached (see Fig. 2c), so-called "sub-resonant operation mode" [3]. After the resonant pulse is completed, the relatively small transformer magnetizing current i_{mag} continues to flow through the previously conductive semiconductors. If the magnetizing current is sufficiently large, it can be used to charge the output capacitances of the semiconductors and thus achieve zero voltage switching (ZVS) for turn on of the semiconductors (see [1], [7]).

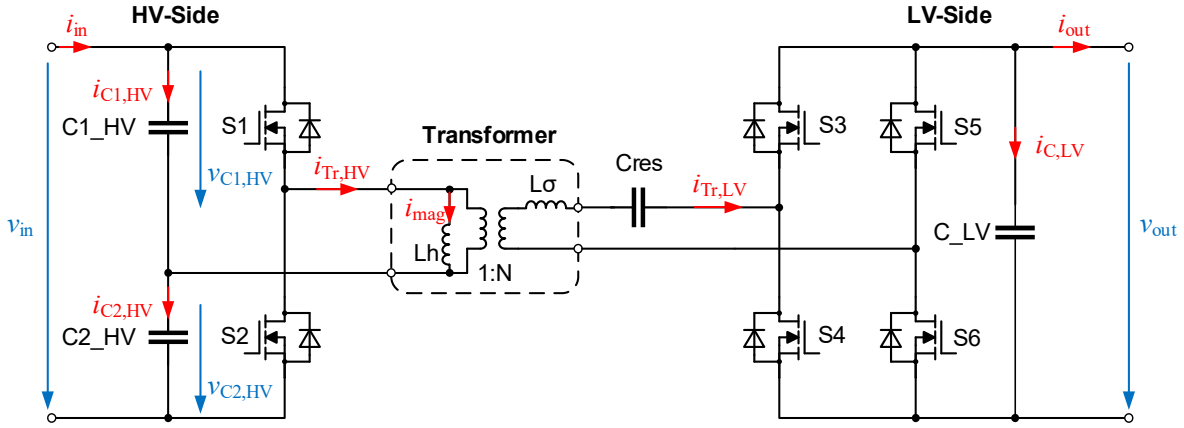

Fig. 1: HB-SRC topology

Due to the very small magnetization inductance L_h of the transformer that is required for this operation, the magnetizing current is limited by the smallest practically feasible inductance value. In order to still be able to provide soft switching when using power modules with large output capacitance values e.g. for high-power applications, a significant dead time between the gate signals of the upper and the lower switches is required. Large parasitic capacitances in the power switches can require a dead time of 10 % or higher in relation to the switching period T_{SW} to achieve proper soft switching operation. This is especially the case for converters that combine high switching frequencies with high output power. Therefore, a significant increase of the resonance frequency in relation to the switching frequency can sometimes be necessary (see Fig. 2c). The resonance tank of the converter, which consists of the resonance capacitance C_{res} and leakage inductance L_σ of the transformer, must be designed accordingly in order to set the desired resonance frequency, as described in [1].
However, increasing the resonance frequency while the switching frequency remains the same affects the shape of the currents through the components of the converter and thus their RMS values and

frequency spectra. This leads to an increased current stress on the capacitors, the transformer and the power semiconductors. Although the power transmitted by the converter remains almost constant, the losses occurring in its components increase. These relationships are examined analytically and through simulations in the following sections.

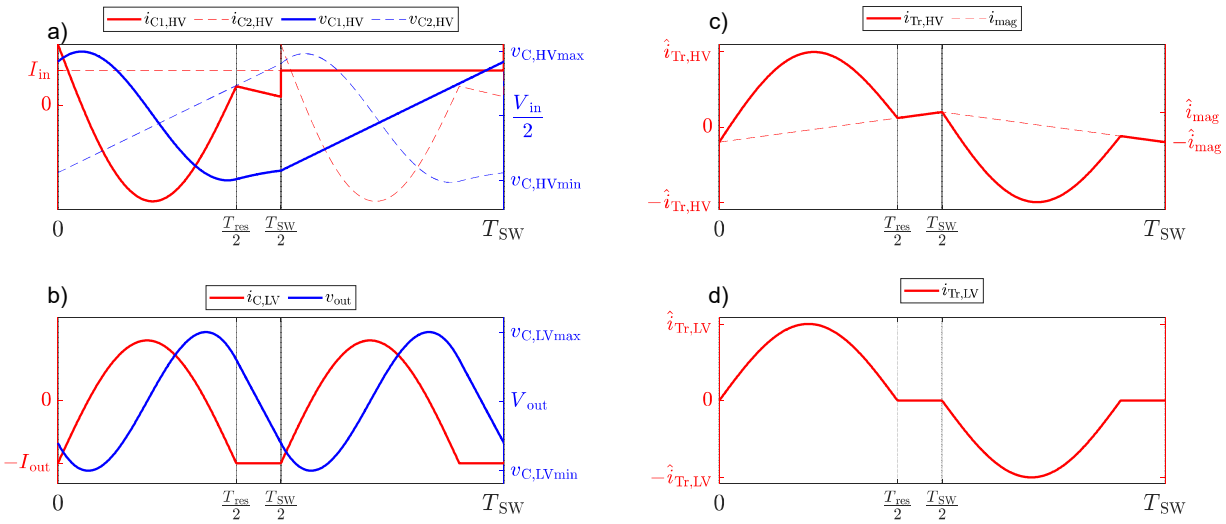

Fig. 2: Typical waveforms (qualitative) of HB-SRC: a) input capacitors (voltages and current), b) output capacitor (voltages and current), c) transformer primary side (current), d) transformer secondary side (current)

Semiconductor loss analysis

To analyze semiconductor losses, an analytical calculation method is derived and validated by simulations using PLECS. Assuming that the primary-side half-bridge always works in soft-switching operation and the secondary-side full bridge works as an ideal synchronous rectifier, consideration of the conduction losses is sufficient.

Table I: Simulation Parameters

Input voltage V_{in}	1900 V
Output voltage V_{out}	665 V
Output power P_{out}	250 kW
Switching frequency f_{SW}	50 kHz
Junction temperature T_j	125 °C

Using the waveform of the currents flowing throw the MOSFETs of the HV-Side (Fig. 3 left) and the LV-Side (Fig. 3 right), RMS values of these currents can be calculated analytically according to (1) and (3). With these RMS values, the conduction losses of the HV-Side and LV-Side MOSFETs could be calculated using (2) and (4), respectively. Note that the magnetization current i_{mag} is neglected for these calculations.

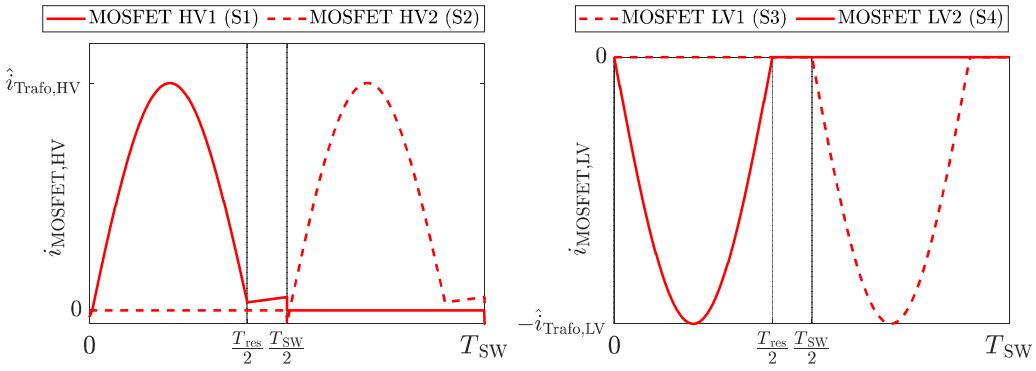

Fig. 3: MOSFET currents HV-Side (left) and LV-Side (right)

In Fig. 4 a) and c), calculated and simulated conduction losses for an application example of an HB-SRC for an electrified wired agricultural machinery presented in [5] are shown. The system parameters used are summarized in Table I and correspond to the application in [5]. In this application, SiC MOSFETs are used both on the primary side and on the secondary side. Energy flows from the HV-Side to the LV-Side of the converter.

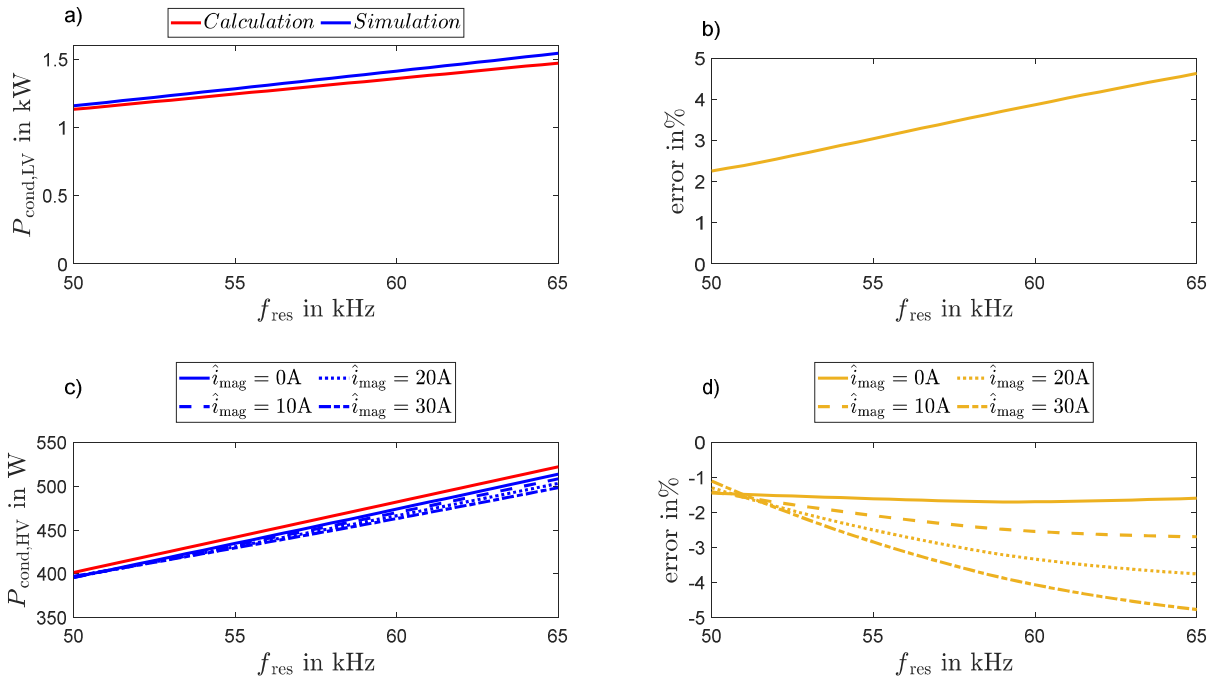

Fig. 4: Calculated and simulated conduction losses vs. resonance frequency f_{res}: a) HV-Side, b) HV-Side calculation error c) LV-Side and d) LV-Side calculation error

Fig. 4 shows the simulated power loss for the HV-Side (c) and the LV-Side (a). It can be seen that the conduction losses increase almost linearly with the resonance frequency for the HV-Side as well as for the LV-Side of the converter. This is true for both the calculated (red) and simulated (blue) conduction losses. For a general overview, the quantitative behavior of the losses is first described using the calculated values, before the deviations between the calculation and the simulation are discussed.

For example, with an increase of the resonance frequency f_{res} from 54 kHz to 62.5 kHz (15.7 %), the calculated conduction losses increase from 434 W to 502 W for the HV-Side module and from 1.224 kW to 1.417 kW for both LV-Side modules. This results in an increase in semiconductor conduction losses of 15.6 % and 15.8 %, respectively, for the same output power of the converter.

As shown in detail in Fig. 4 b) and d), there is a deviation between the calculation and the simulation. On the LV-Side, this is mainly due to the fact that the $R_{DS,on}$ used in the simulation is not constant but depends on the current through the respective MOSFET, which in this case leads to a higher calculation error as the resonance frequency increases. This is due to the fact that the amplitude of the current through the MOSFET increases with increasing resonance frequency and the deviation between the constant $R_{DS,on}$ used in the calculation and the $R_{DS,on}$ curve used in the simulation increases. This means that, for example, the error increases from 2.88 % at a resonance frequency of 54 kHz to 4.26 % at 62.5 kHz.

For the HV-Side however, neglecting the magnetization current i_{mag} leads to an additional error. The simulated losses for different magnetizing currents are compared with the calculated ones in Fig. 4 c). The corresponding calculation error can be seen in Fig. 4 d). With no magnetizing current ($\hat{\imath}_{\mathrm{mag}}$ = 0 A), the cause of the deviation is the same as for the LV-Side. However, an increasing magnetizing current leads to higher calculation errors. For example, with a resonance frequency of 62.5 kHz and a magnetizing current amplitude $\hat{\imath}_{\mathrm{mag}}$ of 30 A, this leads to a deviation of -4.46 %, while without magnetizing current the calculation error is -1.66 %.

$$I_{\mathrm{MOSFET,HV\,RMS}} = \sqrt{\frac{1}{T_{\mathrm{SW}}} \cdot \int_0^{T_{\mathrm{SW}}} i_{\mathrm{MOSFET,HV}}^2 \, dt} = I_{in} \cdot \frac{\pi}{2} \cdot \sqrt{\frac{f_{\mathrm{res}}}{f_{\mathrm{SW}}}}$$
$$\text{with } i_{\mathrm{MOSFET,HV}} = \begin{cases} \hat{\imath}_{\mathrm{Tr,HV}} \cdot \sin(\omega_{\mathrm{res}} \cdot t) \;, & 0 < t \leq \frac{T_{\mathrm{res}}}{2} \\ 0 \;, & \frac{T_{\mathrm{res}}}{2} < t \leq \frac{T_{\mathrm{SW}}}{2} \end{cases} \tag{1}$$

$$P_{\mathrm{cond,HV}} = 2 \cdot R_{\mathrm{DSon,HV}} \cdot I_{\mathrm{MOSFET,HV\,RMS}}^2 \tag{2}$$

$$I_{\mathrm{MOSFET,LV\,RMS}} = \sqrt{\frac{1}{T_{\mathrm{SW}}} \cdot \int_0^{T_{\mathrm{SW}}} i_{\mathrm{MOSFET,LV}}^2 \, dt} = I_{out} \cdot \frac{\pi}{4} \cdot \sqrt{\frac{f_{\mathrm{res}}}{f_{\mathrm{SW}}}}$$
$$\text{with } i_{\mathrm{MOSFET,LV}} = \begin{cases} -\hat{\imath}_{\mathrm{Tr,LV}} \cdot \sin(\omega_{\mathrm{res}} \cdot t) \;, & 0 < t \leq \frac{T_{\mathrm{res}}}{2} \\ 0 \;, & \frac{T_{\mathrm{res}}}{2} < t \leq \frac{T_{\mathrm{SW}}}{2} \end{cases} \tag{3}$$

$$P_{\mathrm{cond,LV}} = 4 \cdot R_{\mathrm{DSon,LV}} \cdot I_{\mathrm{MOSFET,LV\,RMS}}^2 \tag{4}$$

Analytical Calculation of Passive Components Current Stress

The waveforms of the currents through the passive components (Fig. 2) are used for the analytical determination of the RMS current load and the frequency spectra of the component currents. The magnetization current i_{mag} of the transformer can usually be neglected in high-power applications due to its small magnitude compared to the current through the transformer.

$$I_{\mathrm{C1,HV\,RMS}} = I_{\mathrm{C2,HV\,RMS}} = I_{\mathrm{C,HV\,RMS}} = \sqrt{\frac{1}{T_{\mathrm{SW}}} \cdot \int_0^{T_{\mathrm{SW}}} i_{\mathrm{C1,HV}}^2 dt} = I_{in} \cdot \sqrt{\frac{\pi^2}{4} \cdot \frac{f_{\mathrm{res}}}{f_{\mathrm{SW}}} - 1}$$

$$\text{with } i_{\mathrm{C1,HV}} = \begin{cases} I_{\mathrm{in}} - \hat{\imath}_{\mathrm{Tr,HV}} \cdot \sin(\omega_{\mathrm{res}} \cdot t), & 0 < t \leq \frac{T_{\mathrm{res}}}{2} \\ I_{\mathrm{in}}, & \frac{T_{\mathrm{res}}}{2} < t \leq T_{\mathrm{SW}} \end{cases} \tag{5}$$

$$\hat{\imath}_{\mathrm{C1,HV}}(n) = \hat{\imath}_{\mathrm{C2,HV}}(n) = \hat{\imath}_{\mathrm{C,HV}}(n) = 2 \cdot I_{\mathrm{in}} \cdot \frac{\cos\left(\frac{\pi}{2} \cdot n \cdot \frac{f_{\mathrm{sw}}}{f_{\mathrm{res}}}\right)}{\left(n \cdot \frac{f_{\mathrm{sw}}}{f_{\mathrm{res}}}\right)^2 - 1} \tag{6}$$

The analytical expressions used to calculate the RMS values and the frequency spectra of the currents through the components the general equations for calculating a currents RMS value and the Fourier analysis of periodic signals according to [8] are applied to the current waveforms in Fig. 2. This enables the calculation of the RMS values and the frequency spectra of the current for the input capacitors according to (5) and (6), for the transformer (secondary side) according to (7) and (8) and for the output capacitor according to (9) and (10). It should be noted that the RMS values of the primary and secondary transformer currents differ only by the ratio of the input and output currents of the converter, while the frequency spectra only differ through the transformers turn ratio (when the magnetization current i_{mag} is neglected, as mentioned before). Therefore, it is sufficient to discuss the transformers secondary side current here.

$$I_{\mathrm{Tr,LV\,RMS}} = \sqrt{\frac{1}{T_{\mathrm{SW}}} \cdot \int_0^{T_{\mathrm{SW}}} i_{\mathrm{Tr,LV}}^2 \, dt} = \sqrt{\frac{2}{T_{\mathrm{SW}}} \cdot \int_0^{\frac{T_{\mathrm{SW}}}{2}} i_{\mathrm{Tr,LV}}^2 \, dt} = I_{out} \cdot \sqrt{\frac{\pi^2}{8} \cdot \frac{f_{\mathrm{res}}}{f_{\mathrm{SW}}}}$$

$$\text{with } i_{\mathrm{Tr,LV}} = \begin{cases} \hat{\imath}_{\mathrm{Tr,LV}} \cdot \sin(\omega_{\mathrm{res}} \cdot t), & 0 < t \leq \frac{T_{\mathrm{res}}}{2} \\ 0, & \frac{T_{\mathrm{res}}}{2} < t \leq \frac{T_{\mathrm{SW}}}{2} \end{cases} \tag{7}$$

$$\hat{\imath}_{\mathrm{Tr,LV}}(n) = I_{\mathrm{out}} \cdot \frac{\sin\left(\frac{\pi}{2} \cdot n \cdot \left(\frac{f_{\mathrm{sw}}}{f_{\mathrm{res}}} + 1\right)\right) - \sin\left(\frac{\pi}{2} \cdot n \cdot \left(\frac{f_{\mathrm{sw}}}{f_{\mathrm{res}}} - 1\right)\right)}{\left(n \cdot \frac{f_{\mathrm{sw}}}{f_{\mathrm{res}}}\right)^2 - 1} \tag{8}$$

In Fig. 5 a) and b), the RMS values of the currents through the passive components are normalized to the input current i_{in} and the output current i_{out} of the converter, respectively, and plotted over the ratio of the resonance frequency f_{res} and the switching frequency f_{SW}. It can be seen that all current RMS values increase with an increasing ratio of resonance frequency to switching frequency. For example, if this ratio is increased from 1.05 to 1.3 (23.8 % increase), the RMS value of the current through the capacitors on the HV-Side normalized to the input current i_{in} increases by 17.8 % and for the transformer current normalized in the same way by 11.3 %. For the transformer current of the secondary side, normalized to the output current i_{out} of the converter, this leads to an increase of 11.3 %, while the LV-Side capacitor's normalized current increases by 43 %. It should be noted that the ohmic losses occurring in the components depend on the square of the RMS values of the currents (frequency dependency neglected) and thus even relatively small increases lead to an even higher increase in losses.

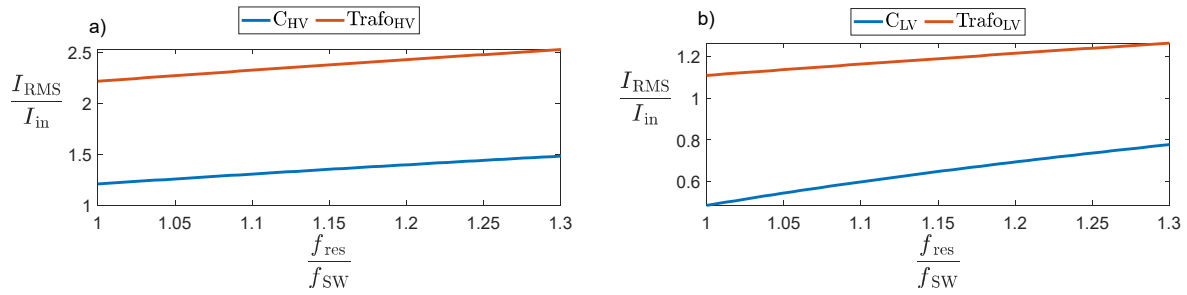

Fig. 5: Component RMS current vs. the ratio of f_{res} and f_{SW}: a) capacitor and transformer HV-Side, b) transformer and capacitor LV-Side

However, since the losses occurring in the passive components depend on the spectra of the currents (see [9], [11]), it is also necessary to consider the change of the spectra when the resonance frequency is increased. In particular, this effect applies to the transformer ([10], [11]). In Fig. 6 a) to c), the three most dominant harmonics, in the respective component currents are plotted over the ratio of resonance frequency f_{res} to switching frequency f_{SW}. In the current through the capacitors on the HV-Side, both even and odd harmonics occur, which all increase with increasing resonance frequency (Fig. 6 a)). Only odd harmonics occur in the transformer currents (Fig.6 b)). In particular, the third and fifth harmonics rise massively with increasing resonance frequency over the shown range. In the current through the capacitor on the LV-Side, only even harmonics appear (Fig. 6 c)).
In the area shown, only the first harmonic increases while the fourth and sixth harmonic even partially decrease.

$$I_{\mathrm{C,LV\,RMS}} = \sqrt{\frac{1}{T_{\mathrm{SW}}} \cdot \int_0^{T_{\mathrm{SW}}} i_{\mathrm{C,LV}}^2 \, dt} = \sqrt{\frac{2}{T_{\mathrm{SW}}} \cdot \int_0^{\frac{T_{\mathrm{SW}}}{2}} i_{\mathrm{C,LV}}^2 \, dt} = I_{out} \cdot \sqrt{\frac{\pi^2}{8} \cdot \frac{f_{\mathrm{res}}}{f_{\mathrm{SW}}} - 1}$$

$$\text{with } i_{\mathrm{C,LV}} = \begin{cases} \hat{\imath}_{\mathrm{Tr,LV}} \cdot \sin(\omega_{\mathrm{res}} \cdot t) - I_{\mathrm{out}}, & 0 < t \leq \frac{T_{\mathrm{res}}}{2} \\ -I_{\mathrm{out}}, & \frac{T_{\mathrm{res}}}{2} < t \leq \frac{T_{\mathrm{SW}}}{2} \end{cases} \tag{9}$$

$$\hat{\imath}_{\mathrm{C,LV}}(n) = 2 \cdot I_{\mathrm{out}} \cdot \frac{\cos\left(\pi \cdot n \cdot \frac{f_{\mathrm{sw}}}{f_{\mathrm{res}}}\right)}{\left(2 \cdot n \cdot \frac{f_{\mathrm{sw}}}{f_{\mathrm{res}}}\right)^2 - 1} \tag{10}$$

As shown for the semiconductor losses, there is also a deviation between simulation and calculation for the passive component of the HV-Side due to the neglected magnetizing current. This affects the calculations of the RMS values and spectra of the HV-Side capacitors as well as the transformer's primary side currents.
To classify this calculation error quantitatively, numerical simulations in PLECS were carried out, again using the application example of an HB-SRC for an electrified wired agricultural machinery, in which $\hat{\imath}_{\mathrm{mag}}$ was varied between 0 A and 30 A in 10 A steps. The resulting absolute (left) and relative (right) errors between simulations and calculations are shown in Fig. 7 for the RMS values (a) and the most dominant harmonics (b - c) of HV-Side transformer and capacitor currents.
As shown in Fig. 7, in case of no magnetization current ($\hat{\imath}_{\mathrm{mag}}$ = 0 A) the calculation error is zero for the whole investigated range of f_{res}, which is true for the RMS values as well as for the harmonics shown. Thus, it can be assumed that the calculation error is only caused by neglecting the magnetization current.

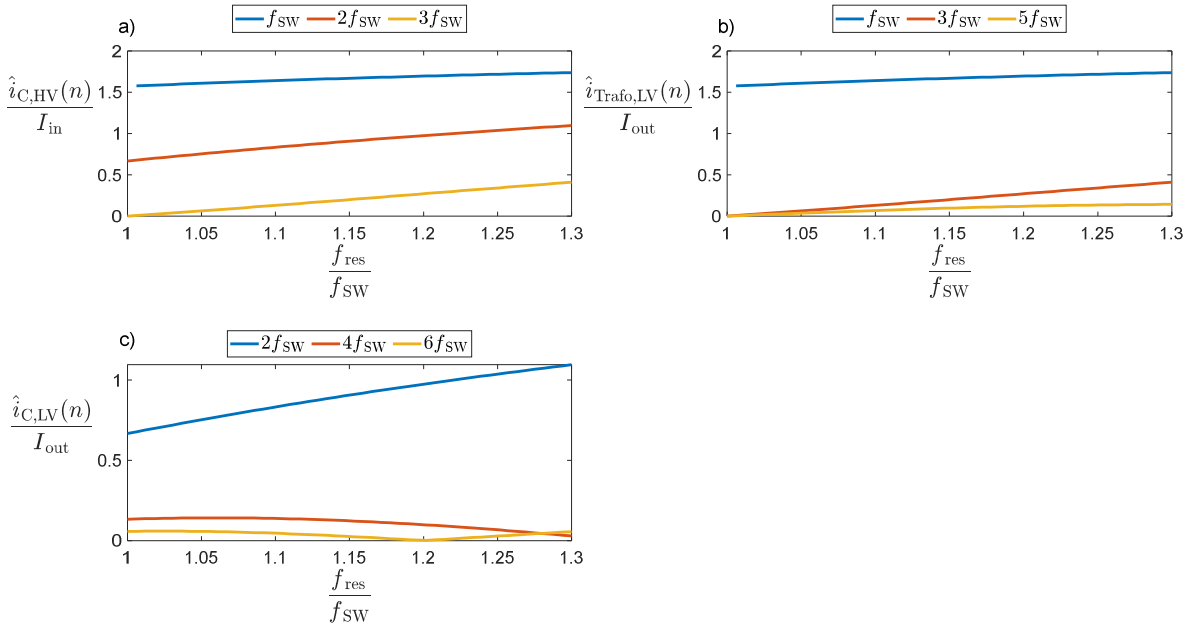

Fig. 6: Component current harmonics vs. the ratio of f_{res} and f_{SW}: a) capacitor HV-Side, b) transformer LV-Side, c) capacitor LV-Side

In Fig. 7 a) and b), the absolute and relative calculation errors of the RMS values and the first harmonics are plotted. For ratios of resonance frequency to switching frequency slightly above unity (approx. 1.05), the calculation error is positive and decreases to negative values with increasing resonance frequency f_{res} for both the transformer and capacitor currents (RMS values and first harmonic). With higher values of the magnetizing current amplitude $\hat{\imath}_{mag}$, the calculation error also increases, and this time almost linearly. Both observations also apply to the second harmonic of the capacitor current shown in Fig. 7 c).
For the third and the fifth harmonic of the transformer current as well as the third harmonic of the capacitor current, the calculation error is positive over the whole investigated range, as shown in Fig. 7 c) and d). First, the absolute error decreases to a minimum near the switching frequency ($f_{SW}/f_{res} = 1$) and then increases again with increasing resonance frequency, but with a declining slope. This leads to an approximately hyperbolic relative error curve.

Minimum required Capacitance for input and output Capacitor

The minimum capacitance required in order to not exceed a certain voltage ripple for both the input and the output side is a function of the switching and resonance frequency as well as the maximum power transmitted by the converter. The shifted charge can be calculated by integrating the current through the respective capacitor (see Fig. 2 a) and b)). For a specified voltage ripple, the minimum capacitance required for the capacitors on the HV- and LV-Side side can be calculated according to (11) and (12), respectively.

$$C_{HV} = \frac{\Delta Q_{C,HV}}{\Delta V_{C,HV}} = \frac{I_{in,max}}{\Delta V_{C,HV}} \cdot \left[\frac{1}{f_{SW}} \cdot \sqrt{1 - \left(\frac{1}{\pi} \cdot \frac{f_{SW}}{f_{res}} \right)^2} - \frac{1}{2 \cdot f_{res}} + \frac{1}{\pi \cdot f_{res}} \arcsin\left(\frac{1}{\pi} \cdot \frac{f_{sw}}{f_{res}} \right) \right] \tag{11}$$

$$C_{LV} = \frac{\Delta Q_{C,LV}}{\Delta V_{out}} = \frac{I_{out,max}}{2 \cdot \Delta V_{out}} \cdot \left[\frac{1}{f_{SW}} \cdot \sqrt{1 - \left(\frac{2}{\pi} \cdot \frac{f_{SW}}{f_{res}} \right)^2} - \frac{1}{f_{res}} + \frac{2}{\pi \cdot f_{res}} \arcsin\left(\frac{2}{\pi} \cdot \frac{f_{sw}}{f_{res}} \right) \right] \tag{12}$$

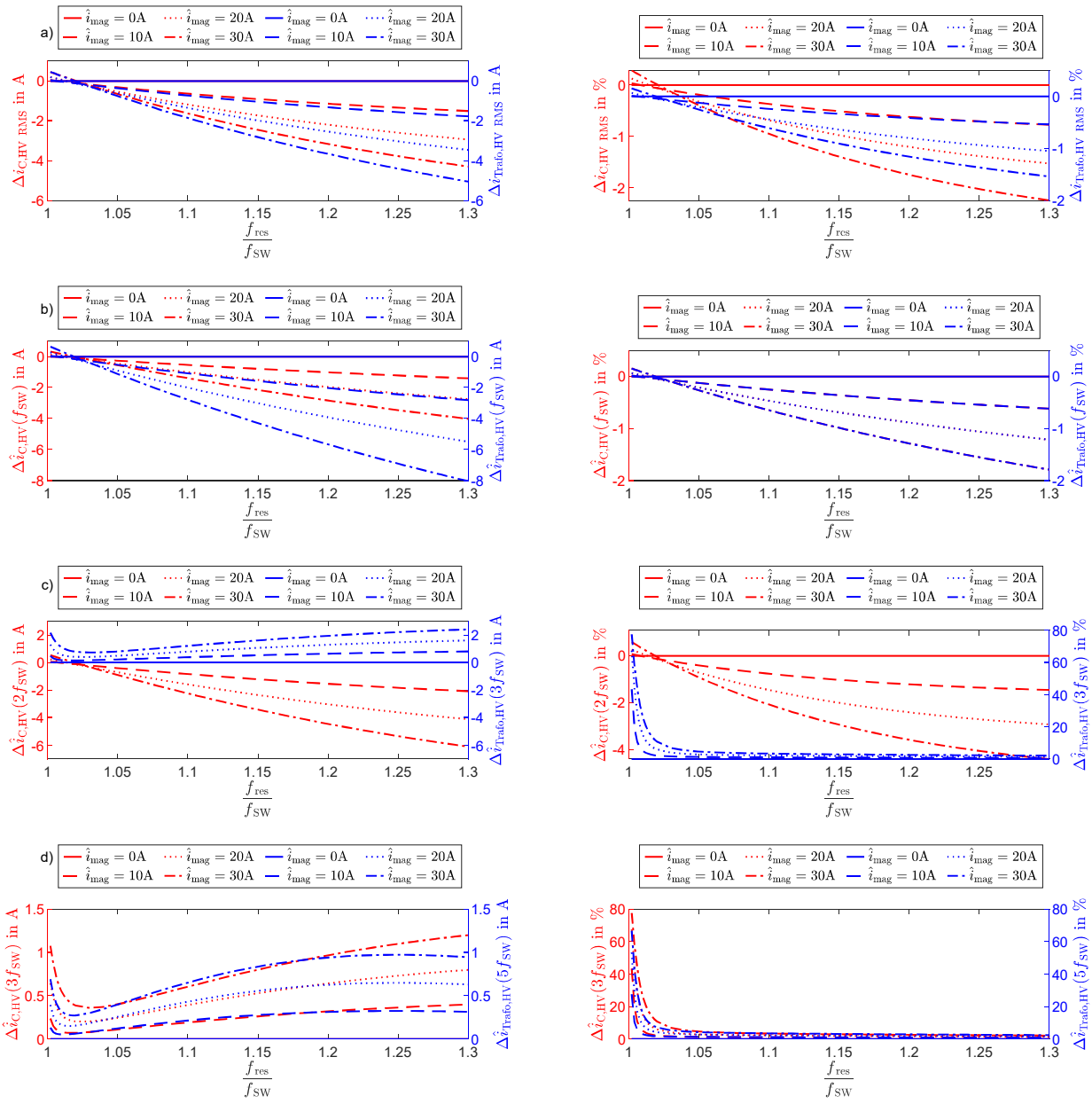

Fig. 7: Calculation error HV-Side capacitor and transformer vs. the ratio of f_{res} and f_{SW} ($I_{\mathrm{out}} = 376$ A): a) RMS values, b) first harmonic (f_{SW}) c) capacitor second harmonic ($2f_{\mathrm{SW}}$) and transformer third harmonic ($3f_{\mathrm{SW}}$), d) capacitor third harmonic ($3f_{\mathrm{SW}}$) and transformer fifth harmonic ($5f_{\mathrm{SW}}$)

Conclusion

The influence of the ratio of the resonance frequency and the switching frequency on semiconductor conduction losses and component current stress in the discontinuous conduction mode (sub-resonant operation mode) of the HB-SRC has been investigated. For this purpose, the analytical equations to determine the semiconductor conduction losses as well as the RMS current loads and the frequency spectra of the respective currents in the passive components have been derived and analyzed. The calculation errors have been investigated for an application example using numerical simulations. Furthermore, analytical equations to calculate the minimum necessary capacitance values for the capacitors on the HV- and LV-Side were derived.

References

[1] D. Rothmund, J. Huber, J. Kolar: “Operating Behavior and Design of the Half-Cycle Discontinuous-Conduction-Mode Series-Resonant Converter with Small DC Link Capacitors”, 2013 IEEE 14th Workshop on Control and Modeling for Power Electronics (COMPEL)

[2] R. Unruh, F. Schafmeister, N. Fröhleke, J. Böckler: “MMC-Topology for High-Current and Low-Voltage Applications with Minimal Number of Submodules, Reduced Switching and Capacitor Losses”, 2019 PCIM Europe

[3] G. Ortiz, H. Uemura, D. Bortis, J. Kolar, O. Apeldoorn: “Modeling of Soft-Switching Losses of IGBTs in High-Power High-Efficency Dual-Active-Bridge DC/DC Converters”, in IEEE Transactionson Electron Devices, VOL. 60, NO. 2, February 2013

[4] C. Stackler, A. Fouineau, P. Ladoux, F. Morel, F. Wallart, P Dworakowski, N. Evans: “NPC assessment in insulated DC/DC converter topologies using SiC MOSFETs for Power Electronic Traction Transformer”, 2019 20th International Symposium on Power Electronics (Ee)

[5] D. Tatusch, A. Gorodnichev, D. Haake, F. Schnabel, J. Friebe, M. Jung: “Hardware and control design considerations for a mobile 1 MW Input-Series Output-Parallel (ISOP) DC-DC converter in Medium Voltage range”, IEEE Energy Conversion Congress and Expo 2021 (ECCE 2021)

[6] T. Guillod, D. Rothmund, J. W. Kolar: “Active Magnetizing Current Splitting ZVS Modulation of a 7 kV/400 V DC Transformer”, IEEE Transactions on Power Electronics, VOL 35, No. 2, February 2020

[7] J. Huber, G. Ortiz, F. Krismer, N. Widmer, J. W. Kolar: “η-ρ Pareto Optimization of Bidirectional Half-Cycle Discontinuous-Conduction-Mode Series-Resonant DC/DC Converter with Fixed Voltage Transfer Ratio”, 2013 Twenty-Eighth Annual IEEE Applied Power Electronics Conference and Exposition (APEC)

[8] F. Zach: “Leistungselektronik: Ein Handbuch Band 1”, 4. Auflage, 2010 Springer

[9] Y. Yang, K. Ma, H. Wang, F. Blaabjerg: “Instantaneous thermal modeling of the DC-link capacitor in PhotoVoltaic systems”, 2015 IEEE Applied Power Electronics Conference and Exposition (APEC)

[10] N. Kimura, K. Nakao, T. Morizane: “Loss Analysis and Temperature Measurement of Middle Frequency Transformer Applied for Solid State Transformer”, 2019 8th International Conference on Renewable Energy Research and Applications (ICRERA)

[11] S. Wang, D. Dorell: “Copper Loss Analysis of EV Charging Coupler”, IEEE Transactions on Magnetics VOL 51, Issue 11, November 2015